THE JOURNAL OF PHYSICAL CHEMISTRY C

Article

pubs.acs.org/JPCC

Theory of Impedance and Capacitance Spectroscopy of Solar Cells with Dielectric Relaxation, Drift-Diffusion Transport, and Recombination

Juan Bisquert,[†,‡,*] Luca Bertoluzzi,[†] Ivan Mora-Sero,[†] and Germà Garcia-Belmonte[†]

[†]Photovoltaics and Optoelectronic Devices Group, Departament de Física, Universitat Jaume I, Avda Sos Baynat, 12071 Castelló Spain

[‡]Department of Chemistry, Faculty of Science, King Abdulaziz University, Jeddah, Saudi Arabia

Supporting Information

ABSTRACT: Semiconductor photovoltaic devices currently investigated, such as hybrid organic–inorganic lead halide perovskite based solar cells, have shown a high dielectric polarization combined with ambipolar carrier transport. In this work, we present a new model that takes into account both features by combining the classical drift-diffusion equation with a generalized Poisson equation that involves a density and frequency dependent dielectric constant that accounts for the polarization of the medium. We derive the corresponding transmission line (TL) and analyze the associated complex plane impedance spectroscopy (IS) and capacitance spectra. The standard dielectric constant is replaced by the dielectric relaxation element that depends on the frequency, which provides a dielectric relaxation subcircuit in the middle rail of the TL. After simplification of the TL, three arcs can be observed: the first one, at low frequency, is associated with the dielectric relaxation process, the second one, at intermediate frequency, is the drift-diffusion/recombination arc, and the last one, at high frequency, corresponds to the geometric capacitance in parallel with transport resistances for both electrons and holes. In the case in which only two semicircles are observed, the parameters that can be extracted are the recombination and dielectric relaxation resistances along with the chemical and dielectric relaxation capacitances. The density dependent static dielectric constant gives rise to current generators that produce exotic impedance spectra associated with inductive behavior. These results provide a major tool for the determination of physical characteristics of lead halide perovskite solar cells.

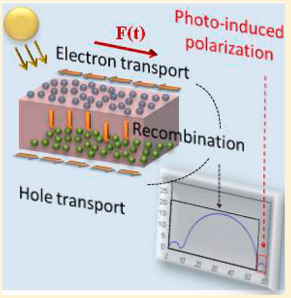

1. INTRODUCTION

Impedance spectroscopy (IS) is a widely used method in the study of the operational mechanisms of different types of solar cells: dye-sensitized solar cells (DSC), organic solar cells, and also in silicon solar cell devices.[1−3] The analysis of solar cells by IS has often been based on a model in which diffusion-recombination of a minority carrier is the dominant phenomenon.[4,5] The solution of this model with the boundary conditions that represent selective contacts gives rise to the popular transmission line (TL) models in which the chemical capacitance plays a central role.[6,7] Especially in DSC it has been often possible to detect a number of distinct features using the TL model: the electron conductivity, chemical capacitance, recombination resistance,[8] as well as the contact effects and conductivity of the electrolyte.[9] The measurement of the equivalent circuit (EC) elements, and their connection to fundamental models of electronic dynamics,[10] has provided a wealth of information about device characteristics and materials operation.

Recently, a new type of organic–inorganic solar cell based on halide perovskite structure has been discovered.[11−14] IS measurement showed that this material displays new properties with respect to the former class of hybrid organic–inorganic materials.[15,16] The hybrid perovskite shows transport of both electrons and holes in the absorber and a very large dielectric polarization that is due to ferroic properties of the perovskite framework.[17,18] This last effect produces a giant dielectric constant that exerts an important influence of the overall dynamic behavior of the cell in the slow time domain and hence dominates the low frequency range of the impedance spectra.[19]

Dielectric polarization introduces a new capacitance in the model that is distinct to the chemical capacitance. This feature has been described many years ago in ac circuits in solid-state electronics[20] as well as in electrochemistry models.[21−23] Both types of approaches have led to the same conclusion that high frequency dielectric polarization is described through a TL EC that includes an additional middle rail containing dielectric capacitors, associated with the geometric capacitance of the material.

So far, however, models have only considered the inclusion of the high frequency polarization through a geometric dielectric constant, ε_∞, that represents orientational polarization and determines the local spatial charge separation through Poisson equation. According to recent findings we

Received: July 28, 2014
Revised: July 29, 2014
Published: July 30, 2014

   dx.doi.org/10.1021/jp5062144 | J. Phys. Chem. C 2014, 118, 18983−18991

need to treat the more general case where dielectric relaxation consists on frequency (ω) dependent polarization.[19] Then it is well-known[24,25] that the complex dielectric constant varies from the low frequency (static) value ε_s to the high frequency (geometric) value ε_∞. A simple type of relaxation is given by the Cole−Cole relaxation peak that takes the form:

$$\varepsilon(\omega) = \frac{\varepsilon_s - \varepsilon_\infty}{1 + (i\omega\tau_{dr})^{1-\alpha}} + \varepsilon_\infty \tag{1}$$

where τ_{dr} is a constant relaxation time and α is a parameter that takes into account the dispersion of relaxation times. For $\alpha = 0$, eq 1 reduces to the case of the Debye relaxation peak for a single relaxation time. Equation 1 is represented as an EC in Figure 1a for the general case of the Cole−Cole dielectric relaxation and in Figure 1b for the case of the Debye relaxation ($\alpha = 0$).

Obviously the presence of the dielectric relaxation introduces additional processes in the solar cell ac impedance behavior, in addition to the classical resistances for transport and recombination, as well as the chemical and contact capacitances.

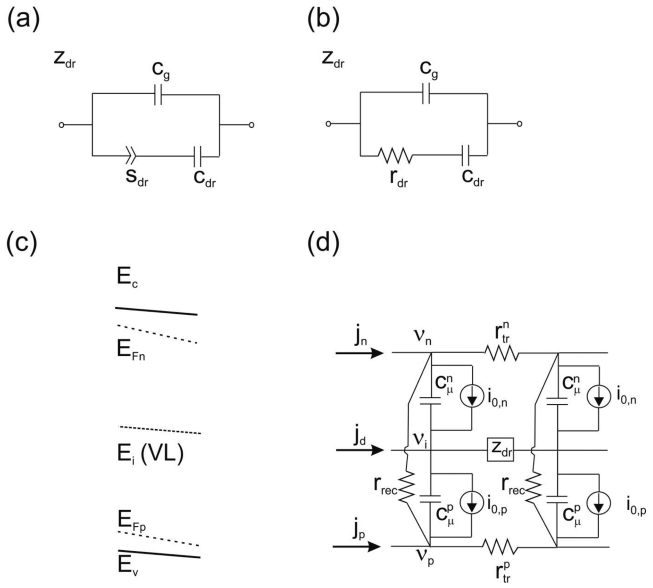

Figure 1. (a) Equivalent circuit representation of the Cole−Cole dielectric relaxation corresponding to eq 1. c_g ($c_g = \varepsilon_\infty$) is the geometric capacitance, c_{dr} ($c_{dr} = \varepsilon_s - \varepsilon_\infty$) is the capacitance associated with the dielectric relaxation, and s_{dr} ($s_{dr} = r_{dr}^{\alpha-1}c_{dr}^{\alpha}$) is the constant phase element (CPE) associated with the Cole−Cole dielectric relaxation, with the impedance $z_\alpha = s_{dr}(i\omega)^{-\alpha}$. (b) Case where $\alpha = 0$ in eq 1, in which the Cole−Cole relaxation time reduces to a single Debye relaxation time and the CPE, s_{dr}, reduces to the dielectric relaxation resistance, r_{dr}. (c) Energy diagram for a semiconductor with transport of electrons in the conduction band with energy E_c and Fermi level E_{Fn}, and transport of holes in the valence band with energy E_v and Fermi level E_{Fp}. The central line corresponds to the intrinsic level E_i that is parallel to the local vacuum level (VL) and represents the bands tilting that arises from the local electrical field. (d) Transmission line (TL) representation of the overall electrical behavior of the semiconductor material in ac mode. The transport lines take conduction current for electrons and holes (j_n, j_p), and the central line takes the displacement current j_d. These lines contain transport resistances r_{tr} for both carriers and local potentials ν_n, ν_p, and ν_i. The vertical lines in the TL contain a recombination resistance r_{rec} and the usual chemical capacitances c_μ for electrons and holes in parallel with the current sources $i_{0,n}$ for electrons and $i_{0,p}$ for holes. The central line contains Z_{dr}, the general Cole−Cole dielectric relaxation EC shown in (a).

In this paper, we formulate the theory for electrons and holes transport coupled with recombination and the generalized Poisson equation that takes into account a density and frequency dependent dielectric relaxation. We derive the small perturbation equations in terms of local electrochemical potentials and potential of the intrinsic level and recover the general transmission line model. We show that dielectric relaxation represented by eq 1 introduces a number of totally new aspects to the TL response of solar cells. We present an analysis of the main features that can be expected in the IS spectra under the influence of these phenomena. We also highlight the cases in which distinct new features of the model have been already observed and reported in the literature. A comprehensive experimental analysis of perovskite solar cells by application of the model will be presented in future work.

2. THE MODEL EQUATIONS

To develop our IS model, we start from a standard model for a semiconductor that contains electrons and holes as shown in Figure 1c. In the following, we formulate the equations that describe transport, recombination, and polarization at any point in the bulk material. In the next section, we will derive the expression for ac modulated small perturbations.

We assume a density of electrons n in the conduction band at the energy E_c and effective density of states (DOS), N_c. n depends on the Fermi level, E_{Fn}, position in the band gap. Similarly, we consider a density of holes p in the valence band at the energy E_v, with effective DOS N_v and Fermi level E_{Fp}. For a nondegenerated semiconductor, the densities of electrons and holes can be written in terms of the Fermi levels through Boltzmann statistics:

$$n = n_i e^{(E_{Fn} - E_i)/k_B T} \tag{2}$$

$$p = p_i e^{-(E_{Fp} - E_i)/k_B T} \tag{3}$$

where

$$n_i = N_c e^{(E_i - E_c)/k_B T} \text{ and } p_i = N_v e^{(E_v - E_i)/k_B T} \tag{4}$$

Here E_i is the intrinsic level defined below, the energy gap is $E_g = E_c - E_v$ and $k_B T$ is the thermal energy.

The carrier densities are modulated by the local electric field F through the Poisson equation:

$$\frac{\partial D}{\partial x} = q\rho \tag{5}$$

where D is the electric displacement field given by $D = \varepsilon F$, q is the elementary charge, and ρ is the local charge density. The static value of the dielectric constant depends on the carrier concentration[19] and takes the form $\varepsilon_s = \varepsilon_s(n, p)$.We assume a p-doped semiconductor (in which holes are majority carriers) with constant density of negatively ionized acceptor centers N_A. The situation of n-doped material is trivially obtained by a change of notation. Thus, we have

$$\rho = p - n - N_A \tag{6}$$

On the one hand, the local electric field F varies with the electric (Galvani) potential φ as

dx.doi.org/10.1021/jp5062144 | J. Phys. Chem. C 2014, 118, 18983−18991

$$F = -\frac{\partial \varphi}{\partial x} \tag{7}$$

On the other hand, φ can be described by the local intrinsic level E_i, defined by the relation $n_i = p_i$

$$E_i = \frac{E_c + E_v}{2} + \frac{1}{2}k_B T \ln\left(\frac{N_v}{N_c}\right) \tag{8}$$

In terms of electron affinity χ_n, we have

$$E_c = -\chi_n - q\varphi \tag{9}$$

$$E_v = -\chi_n - q\varphi - E_g \tag{10}$$

Thereby

$$E_i = -\frac{E_g}{2} - q\varphi - \chi_n + \frac{1}{2}k_B T \ln\left(\frac{N_v}{N_c}\right) \tag{11}$$

Let us now focus on the distribution of local electrical current. The total current has three components, as shown in Figure 1d: conduction currents of electrons and holes and the displacement current:

$$j = j_n + j_p + j_d \tag{12}$$

The conduction currents follow from the drift-diffusion approach:

$$j_n = qnu_n F + qD_n \frac{\partial n}{\partial x} \tag{13}$$

$$j_p = qpu_p F - qD_p \frac{\partial p}{\partial x} \tag{14}$$

Here u_k is the mobility and D_k (k = n,p) is the carrier diffusion coefficient. These two last equations can also be expressed in terms of the carrier conductivities, σ_k, using the classical Einstein relation $D_k = u_k k_B T/q$:

$$j_n = \frac{\sigma_n}{q}\frac{\partial E_{Fn}}{\partial x} \tag{15}$$

$$j_p = \frac{\sigma_p}{q}\frac{\partial E_{Fp}}{\partial x} \tag{16}$$

By introducing the transport resistance for each carrier, $r_{tr}^k = \sigma_k^{-1}$, these two equations can be written as

$$j_n = \frac{1}{q r_{tr}^n}\frac{\partial E_{Fn}}{\partial x} \tag{17}$$

$$j_p = \frac{1}{q r_{tr}^p}\frac{\partial E_{Fp}}{\partial x} \tag{18}$$

These currents are connected to the generation (G) and recombination [$U_r = U_r(n,p)$] processes through the continuity equations:

$$\frac{\partial n}{\partial t} = \frac{1}{q}\frac{\partial j_n}{\partial x} + G - U_r \tag{19}$$

$$\frac{\partial p}{\partial t} = -\frac{1}{q}\frac{\partial j_p}{\partial x} + G - U_r \tag{20}$$

Moreover, the displacement current is

$$j_d = \frac{\partial D}{\partial t} \tag{21}$$

3. SMALL SIGNAL AC PERTURBATION

Let us introduce a small perturbation of the Fermi levels and intrinsic level (modulated by the external voltage):

$$\hat{E}_{Fn} = -q v_n \tag{22}$$

$$\hat{E}_{Fp} = -q v_p \tag{23}$$

$$\hat{E}_i = -q v_i \tag{24}$$

Then, the small perturbation of the carrier densities are

$$\hat{n} = -\frac{c_\mu^n}{q}(v_n - v_i) \tag{25}$$

$$\hat{p} = \frac{c_\mu^p}{q}(v_p - v_i) \tag{26}$$

These equations describe the modulation of the carrier densities by a change of both chemical potentials and the position of the conduction/valence band (by an electric field). In the previous equations, we used the chemical capacitances of free carriers defined by[26]

$$c_\mu^n = q^2\frac{dn}{dE_{Fn}} = \frac{q^2 n}{k_B T} \tag{27}$$

$$c_\mu^p = -q^2\frac{dp}{dE_{Fp}} = \frac{q^2 p}{k_B T} \tag{28}$$

and the recombination resistance, for a band to band recombination rate, is given by

$$r_{rec} = \left(q\frac{dU_r}{dE_{Fn}}\right)^{-1} = \left(-q\frac{dU_r}{dE_{Fp}}\right)^{-1} \tag{29}$$

A more general recombination model via an intermediate defect level has been previously discussed.[26]

The continuity eqs 19−20, combined with eqs 17−18, for small perturbations in the Laplace space, become:

$$\frac{\partial v_n}{\partial x} = -r_{tr}^n i_n \tag{30}$$

$$\frac{\partial v_p}{\partial x} = -r_{tr}^p i_p \tag{31}$$

The previous two equations provide the top and bottom transport rails in the TL as shown in Figure 1d. In addition, we get:

$$\frac{\partial i_n}{\partial x} = -i\omega c_\mu^n(v_n - v_i) - {r_{rec}}^{-1}(v_n - v_p) \tag{32}$$

$$\frac{\partial i_p}{\partial x} = -i\omega c_\mu^p(v_p - v_i) - {r_{rec}}^{-1}(v_p - v_n) \tag{33}$$

and the displacement current small perturbation is obtained through eq 21:

$$i_d = -\frac{1}{z_d}\frac{\partial v_i}{\partial x} - \frac{\gamma_n}{z_d}(v_n - v_i) + \frac{\gamma_p}{z_d}(v_p - v_i) \tag{34}$$

dx.doi.org/10.1021/jp5062144 | J. Phys. Chem. C 2014, 118, 18983−18991

where $z_d = (i\omega\varepsilon(\omega))^{-1}$ and

$$\gamma_n = F\frac{\partial \ln \varepsilon_s}{\partial n}c_\mu^n \tag{35}$$

$$\gamma_p = F\frac{\partial \ln \varepsilon_s}{\partial p}c_\mu^p \tag{36}$$

These two parameters are associated with the density dependent static dielectric constant, $\varepsilon_s = \varepsilon_s(n, p)$, that has been observed in a giant dielectric constant phenomenon in perovskite solar cells.[19] Note that the two last terms of the right-hand side of eq 34 only depend on the voltage applied to the chemical capacitances in the vertical branches but not on the voltage applied to the impedance z_d. These terms are therefore associated with current sources, see Figure 1d. Also note that current sources should appear in parallel with the transport resistances,[27] but we have neglected it here in order to focus on the main purpose of this article: relating polarization with ambipolar transport.

The equivalent circuit, which takes the form of a TL, can hence be recovered through eqs 30−34. The general equivalent circuit for this type of system is given in Figure 1d. Note that for clarity of the scheme, we have used the notations $i_{0,n}$ and $i_{0,p}$ that, respectively, stand for the quantities $\gamma_n/z_d(\nu_n - \nu_i)$ and $\gamma_p/z_d(\nu_p - \nu_i)$. The total impedance of this EC is obtained by solving eqs 30−34:

$$Z(\omega) = \frac{\nu_n(0) - \nu_p(L)}{i_{tot}} \tag{37}$$

The procedure that has been applied to solve these equations is explained in Supporting Information.

4. DISCUSSION

The determination of ac response of our model provides some significant new points with respect to the standard circuit that is given in previous works.[20,23,28] Here the standard dielectric constant is replaced by the dielectric relaxation element that depends on the frequency (eq 1). Therefore, the standard geometric capacitance in the middle rail of the TL is replaced by the relaxation subcircuit of parts a or b of Figure 1, depending on the distribution of relaxation times. This feature is described here for the first time (Figure 1d). In the vertical lines of Figure 1d, we also find classical features of chemical capacitances, c_μ^n and c_μ^p, and recombination resistance r_{rec}. The other new feature is the presence of the current sources in parallel with the chemical capacitances. These components depend on the derivative of the dielectric constant and the local electric field and are only significant in regions where space charge is large. To simplify the discussion, we will consider first the case of a homogeneous distribution of carriers implying a weak electric field and therefore neglect the influence of these current sources. Later on, current sources will be considered and their effect analyzed. The general TL without these elements is given in Figure 2a. Note that this model just describes the active layer, and it does not include additional circuit elements that could be expected in a real device as series resistance or charge transfer at the interface with selective contacts coupled with the interfacial capacitance.[29]

We now analyze the equivalent circuit of Figure 2a for a better understanding of the varied complex plane impedance spectra. To better apprehend the complex circuit of Figure 2a, we proceed to a simplification of the TL where the dielectric

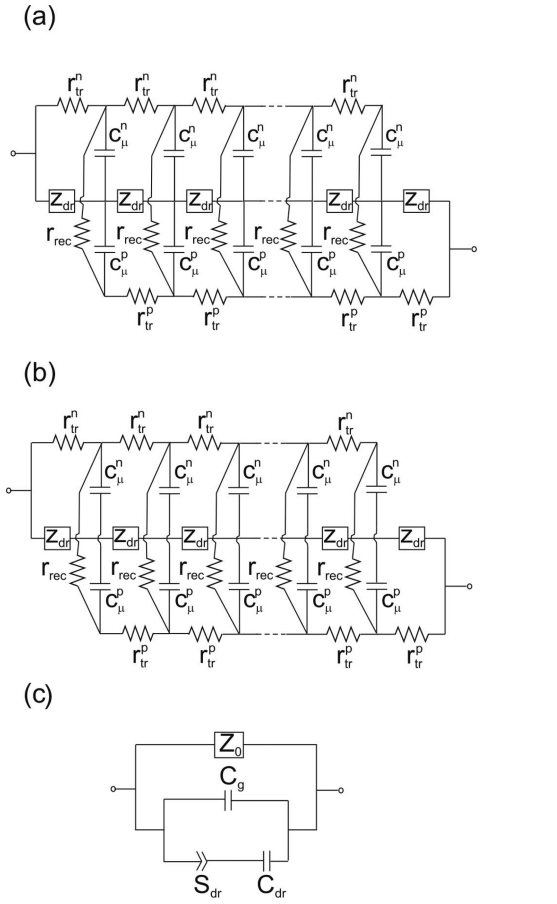

Figure 2. (a) General transmission line (TL) model (extension of Figure 1d) without the current sources. (b) Simplified circuit in which the dielectric relaxation subcircuit has been decoupled from the rest of the transmission line of (a). (c) Equivalent circuit of the circuit given in (b).

relaxation has been decoupled from electronic transport (Figure 2b), as already done in another work.[30] Note that in Figure 2b, the Z_{dr} element is not connected to any of the chemical capacitances. In addition, we assume the local elements of the TL to be constant and position-independent. Note that the resistances r_k and chemical capacitances c_k are local quantities, while R_k and capacitances C_k are their corresponding integrated quantities for the homogeneous case: $R_k = r_k L$ and $C_k = c_k L$, where L is the length of the semiconductor layer. A reduced form of such TL is given in Figure 2c. In the latter circuit, the impedance corresponding to ambipolar transport without the dielectric relaxation subcircuit can be reduced to one single impedance Z_0 that takes the form:

$$Z_0 = \frac{R_{tr}^n R_{tr}^p}{R_{tr}^n + R_{tr}^p}\left[\frac{1}{\Lambda\sinh(\Lambda)}\left[2 + \left(\frac{R_{tr}^p}{R_{tr}^n} + \frac{R_{tr}^n}{R_{tr}^p}\right)\cosh(\Lambda)\right] + 1\right] \tag{38}$$

where

$$\Lambda = \left[\left({R_{rec}}^{-1} + i\omega\frac{C_\mu^n C_\mu^p}{C_\mu^n + C_\mu^p}\right)(R_{tr}^n + R_{tr}^p)\right]^{1/2} \tag{39}$$

dx.doi.org/10.1021/jp5062144 | J. Phys. Chem. C 2014, 118, 18983−18991

In the following, we will write

$$C_{\mu,eq} = \frac{C_\mu^n C_\mu^p}{C_\mu^n + C_\mu^p} \quad (40)$$

The calculation of Z_0 is given in Supporting Information. Note that in the discussion below we assume the chemical capacitances to have similar values.

We comment on the different physical origin of the capacitances that are included in this model. The chemical capacitance of a carrier, C_μ, is due to the displacement of the Fermi level with respect to the respective band edge, and describes accumulation of carriers in the absorber.[6] It is proportional to the volume of material, see the specific capacitance in eq 27, therefore it increases proportionally to the absorber thickness.

On the other hand, a dielectric capacitance is given by the expression

$$C = \frac{\varepsilon_r \varepsilon_0}{L} \quad (41)$$

where ε_r is the relative dielectric constant and ε_0 is the permittivity of the vacuum. The dielectric constant depends on the frequency as stated in eq 1. Thus, at high frequency, the dielectric constant $\varepsilon_\infty = \varepsilon_{r\infty}\varepsilon_0$ determines the geometric capacitance C_g. For many inorganic semiconductors, $\varepsilon_{r\infty} \approx 10$. The low frequency dielectric constant, $\varepsilon_s = \varepsilon_{r,s}\varepsilon_0$, in turn, determines the low frequency capacitance C_{dr}. For the hybrid metal halide perovskites, a very large static dielectric constant, $\varepsilon_{r,s} \approx 10^4$, dependent on illumination and carrier density, has been observed.[19] Because both C_g and C_{dr} comply with eq 41, they must decrease with the thickness of the region that contains the polarization, in contrast to the chemical capacitance. These different dependencies are represented in Figure 2b by the parallel connection of chemical capacitances and series connection of dielectric capacitances.

We examine the most general case of the impedance spectra, shown in Figure 3, where three arcs are displayed in the complex impedance plane (Figure 3b), when $C_g < C_\mu^n$, $C_\mu^p < C_{dr}$ and assuming a single dielectric relaxation time. The complex capacitance is defined from the impedance as follows

$$C^*(\omega) = \frac{1}{i\omega Z(\omega)} \quad (42)$$

It is conventionally separated into real and imaginary part according to the expression[31]

$$C^*(\omega) = C' - iC'' \quad (43)$$

Figure 3c shows the real part of the complex capacitance. The three capacitive features contained in the system are progressively observed in the representation of capacitance as a function of frequency, namely, the geometric capacitance at high frequency, the chemical capacitance at middle frequency, and the static dielectric capacitance at low frequency. Each of these capacitances appears as the respective capacitance step when the correspondent relaxation process is activated in the frequency domain. The steps of the capacitance have been previously observed in $CH_3NH_3PbI_3$ perovskite solar cells.[17] An intuitive interpretation of Figure 3c is as follows. The dielectric capacitance is frequency dependent as stated in eq 1, and it makes a transition from C_g to C_{dr}, as the frequency decreases, due to the polarization and dielectric relaxation properties of the medium. The accumulation of carriers produces an additional effect, the chemical capacitance, that contributes in the medium frequency range, hence the three steps in Figure 3c. However, it must be also noted that the frequency of onset of the capacitance in the system in the frequency axis depends on the resistive properties. Figure 3c is therefore not a general situation. The capacitance and resistive behavior of the system is finally given by the general EC that has been presented in Figure 2a. It is observed that different situations can be expected, and some of them are discussed below. In addition, the values of capacitance may show different ordering due to dependencies commented above. For example, for a dielectric film of $L = 0.5$ μm, with $\varepsilon_{r\infty} = 10$ and $\varepsilon_{r,s} \approx 10^4$, then $C_g = 2 \times 10^{-8}$ F cm^{-2} and $C_{dr} = 2 \times 10^{-5}$ F cm^{-2}. If the density of carriers is 10^{16} cm^{-3}, then $C_\mu = 2 \times 10^{-6}$ F cm^{-2}. The sequence of capacitance steps will be as in Figure 3c. However, a change of thickness, carrier density, and dielectric constant may provide very different results.

Furthermore, the solar cell device may show additional capacitive features, such as depletion layer (associated with band bending), that modifies the geometrical capacitance, contact capacitances at interfaces with the electron and hole transport media, or at current collectors, as mentioned before, and Schottky barriers at grain boundaries.[32]

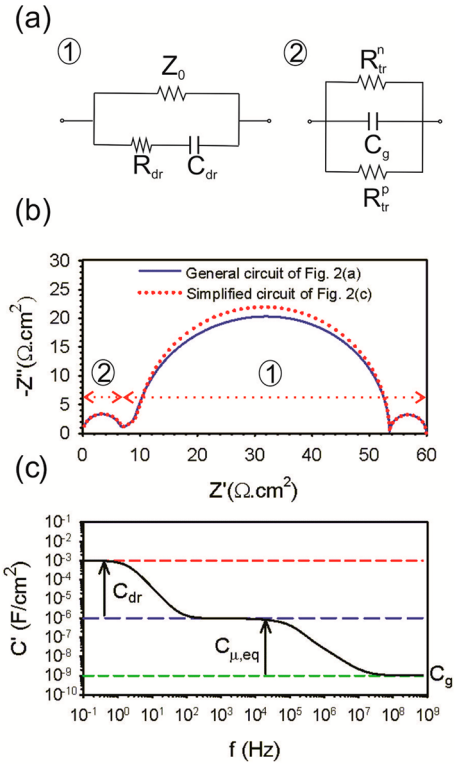

Figure 3. (a) Simplified circuit of Figure 2c calculated for low (1) and high (2) frequencies, considering a single time for the dielectric relaxation (Debye relaxation subcircuit of Figure 1b) (b) General impedance spectra corresponding to the general TL of Figure 2a with a Debye relaxation subcircuit (blue solid line) and the simplified circuit of Figure 2c (red dots). The processes associated with these semicircles are discussed in the main text. (c) Real part of the total capacitance as a function of frequency: at low frequency, the capacitance corresponding to the dielectric relaxation (C_{dr}), at intermediate frequency, both chemical capacitances in series and at high frequency the geometric capacitance (C_g). For these simulations, we used: $C_\mu^n = C_\mu^p = 2 \times 10^{-6}$ F/cm^2, $C_{dr} = 10^{-3}$F/cm^2, $C_g = 10^{-9}$F/cm^2, $R_{tr}^n = 20\cdot\Omega\cdot$cm^2, $R_{tr}^p = 10\Omega\cdot$cm^2, $R_{rec} = 50\Omega\cdot$cm^2, $R_{dr} = 500$ $\Omega\cdot$cm^2.

dx.doi.org/10.1021/jp5062144 | J. Phys. Chem. C 2014, 118, 18983−18991

Even though Figure 2a and the correspondent analytic expression describe the general behavior of impedance and capacitance response of the solar cell, for practical purposes it is very useful to develop simplified models, containing the main physical ingredients that facilitate rapid analysis of data. According to Figure 3b, the simplified EC of Figure 2c is a good approximation to estimate the impedance spectra corresponding to the general TL of Figure 2a. Consequently, we can use the simpler EC of Figure 2c to associate each semicircle with its corresponding physical process.

At low frequency, the impedance associated with the geometric capacitance is negligible and the EC of Figure 2c is reduced to the EC (1) of Figure 3a that is responsible for the two semicircles in the IS spectra observed in the region 1 (Figure 3b). The first arc, at the lowest frequencies, corresponds to the dielectric relaxation process, while the second one is identified to the drift-diffusion/recombination processes. Note that in the example of Figure 3b, the transmission line behavior, the prolongation of the straight line that intersects the middle arc,[4] can be observed because the values of the recombination and transport resistances are chosen such that $r_{rec} > r^{n}_{tr}, r^{p}_{tr}$. If we had chosen $r_{rec} < r^{n}_{tr}, r^{p}_{tr}$ (case of a nonhomogeneous carrier density profile), the IS spectra would instead display a Gerischer behavior, where the prolongation of the straight line does not intersect the recombination arc.[5,15] At high frequencies, the geometric capacitance dominates and Z_0 is reduced to

$$Z_0^{hf} = \frac{R_{eq}}{1 + i\omega R_{eq} C_{\mu,eq}} \tag{44}$$

where R_{eq} is the parallel association of transport resistances:

$$R_{eq} = \frac{R^{n}_{tr} R^{p}_{tr}}{R^{n}_{tr} + R^{p}_{tr}} \tag{45}$$

Hence, the last semicircle at high frequency, region 2 in Figure 3b, can be associated with the geometric capacitance in parallel with the transport resistances (EC (2) of Figure 3a). Note that if one of the carriers has a high conductivity, the associated transport resistance tends to zero and this last arc is not visible in the impedance spectra.

For the sake of practical applications, we shall now discuss the cases of Figure 4 where only two semicircles can be observed. In a high conductivity case, in which either one of the transport resistances for electrons or holes is negligible, the geometric arc will not appear in the IS spectra at high frequency, region 2, Figure 3b. If both transport resistances are small, as in Figure 4, the straight line feature also disappears. We mainly focus on this last case where the Warburg behavior is not visible in the IS spectra. The corresponding simplified EC is depicted in Figure 4a. As expected, this EC can give rise to two arcs, as shown by parts b and c of Figure 4. In both cases, the low frequency arc is the one associated with the dielectric relaxation and the second one to the drift-diffusion/recombination processes. The only difference between parts b and c of Figure 4 is the value of the resistance R_{dr}, which is smaller in Figure 4b than in Figure 4c. Thus, R_{dr} regulates the relative size of both arcs. Note that $Z_0(\omega = 0) = R_{rec}$, as the lower branch of Figure 4a, vanishes at low frequency. Thereby, it is possible to directly extract the resistance R_{rec} from the value of the impedance at zero frequency. An alternative way of obtaining R_{rec}, especially useful when additional features are observed in the complex impedance plot, is to obtain it from

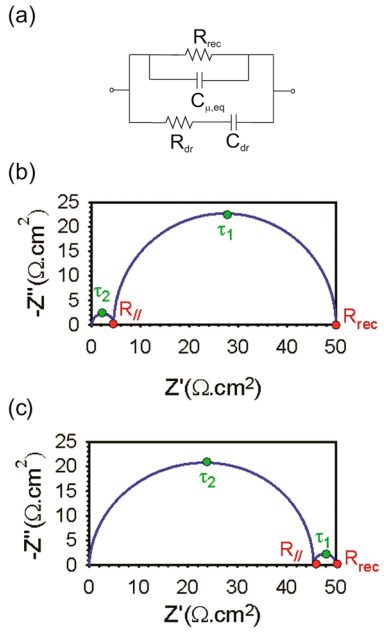

Figure 4. (a) Simplified EC of Figure 2c in the absence of transport resistance ($R^{n}_{tr} = R^{p}_{tr} = 10^{-3}\Omega\cdot cm^2$) and with a single dielectric relaxation time in the framework of the Debye model (Figure 1b). IS spectra for the general TL of Figure 2a for two different cases, small and high dielectric relaxation resistance: (b) $R_{dr} = 5\Omega\cdot cm^2$ and (c) $R_{dr} = 500\Omega\cdot cm^2$. The other parameters take the same values as the ones of Figure 3. The processes associated with each arc as well as the meaning of $R_{\|}$, τ_1, and τ_2 are discussed in the main text.

the sum of the resistances of the two arcs. Note that these resistances individually have no direct physical meaning, only their sum (R_{rec}), and the ratio between both, are controlled by R_{dr}. The other parameters R_{dr}, $C_{\mu,eq}$, and C_{dr} can be obtained through the values $R_{\|}$, τ_1, and τ_2, indicated in Figure 4b,c. Indeed, in the Supporting Information, we show that if $C_{dr} \gg C_{\mu,eq}$:

$$R_{\|} = \frac{R_{rec} R_{dr}}{R_{rec} + R_{dr}} \tag{46}$$

$$\tau_1 = (R_{rec} + R_{dr}) C_{dr} \tag{47}$$

$$\tau_2 = \frac{R_{rec} R_{dr}}{(R_{rec} + R_{dr})} C_{\mu,eq} \tag{48}$$

The analysis of the ac behavior in the frequency domain, can be applied for the interpretation of time transients in the time domain. This topic is beyond the scope of this paper, but we note that the characteristic times given in eqs 47 and 48 largely determine the decay time observed in the time domain. Large capacitances imply long decays when a step perturbation is applied, and this feature has been recently observed.[17] It was also suggested that the capacitive transients introduce significant hysteresis features in current−voltage curves. It is also important to realize that these time constants are influenced by characteristics of the dielectric relaxation process, as C_{dr} and R_{dr}, so that the attribution of recombination times (lifetime) is not straightforward.

So far, we have discussed the case of a single dielectric relaxation time and have adopted the Debye model for the dielectric relaxation (Figure 1b). We shall now discuss the effect of a distribution of relaxation times in the framework of the

dx.doi.org/10.1021/jp5062144 | J. Phys. Chem. C 2014, 118, 18983−18991

Cole−Cole approximation (Figure 1a), mentioned earlier in this paper. This situation corresponds to positive, nonzero values of the parameter α in eq 1. In Figure 5, we present the

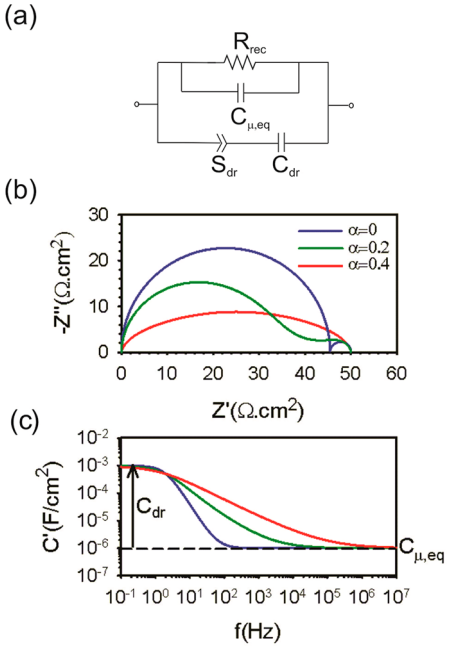

Figure 5. (a) Simplified EC of Figure 2c in the absence of transport resistance and a distribution of dielectric relaxation lifetimes in the framework of the Cole−Cole approximation, Figure 1a. (b) Effect of a distribution of relaxation lifetimes on the complex plane impedance spectra for three different values of the parameter α. Note that the case $\alpha = 0$ corresponds to the case of a single relaxation time of Figure 4c. (c) The associated real part of the total capacitance as a function of the frequency of the small perturbation for the three different values of the parameter α. For these simulations, the parameters are the same than in Figure 4c.

evolution of the IS spectra for three different values of α (Figure 5a) and the evolution of the respective capacitance. As α increases, the distribution of dielectric relaxation lifetimes is broader and the dielectric relaxation occurs at a wider range of frequencies, as displayed by Figure 5b. The chemical capacitance will therefore be observed at higher frequencies, where the impedance tends to zero. Hence at larger values of the parameter α (for the example of Figure 5b, it corresponds to the case $\alpha = 0.4$), the IS spectra display a single elliptic arc which is associated with the polarization with a broad distribution of relaxation lifetimes. Note that in the case of transport limitations, the transmission line behavior could be concealed by the Cole−Cole feature at high frequency.

The last distinctive behavior in the new model that we consider is the presence of current source elements that appear in the general case of Figure 1d. To describe the spectral features caused by these elements, they have been included in the general TL but without transport resistances, and the results are shown in Figure 6. The model predicts that the presence of the current sources could produce exotic behaviors of the impedance spectra. As can be noticed from these plots, current sources are responsible for an inductive behavior at low frequencies (Figure 6a) and even at higher frequencies (Figure 6b). The inductive behavior is well-known in a variety of hybrid organic−inorganic solar cells.[33] These kind of features have been previously reported in perovskite solar cells, an inductive

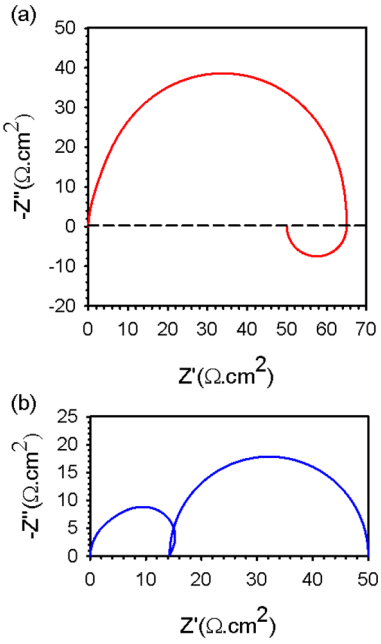

Figure 6. Examples of IS spectra with the presence of the current sources for the general circuit of Figure 1d without transport resistance. Two cases are shown: (a) $\gamma_n = 5$ and $\gamma_p = 1$ (b) $\gamma_n = -1$ and $\gamma_p = -10$.

effect at low frequency,[17] as in Figure 6a, and a loop in the complex impedance plot at intermediate frequencies,[29] as in Figure 6b. It is satisfactory that such widely reported behavior is well explained by a physical model that does not introduce any ad hoc negative capacitance. Further analysis is required to clarify the impact of these features in the cell performance.

5. CONCLUSION

In this work, we have developed a more general transmission line model that takes into account ambipolar characteristics and dielectric relaxation in semiconductor devices for photovoltaic applications. Two new and important features appear in this model: the presence of the frequency and density dependent dielectric constant and the current sources in parallel with the usual chemical capacitance in the vertical branches of the TL. We have first discussed the different features of the possible IS spectra without these current sources. We have demonstrated that, for similar values of the chemical capacitances and in the framework of the Debye dielectric relaxation, three semicircles can be observed in the complex plane IS spectra. These semicircles have been identified by the dielectric relaxation processes as low frequency, drift-diffusion-recombination at intermediate frequencies and the geometric capacitance in parallel with both transport resistances at high frequency. We then analyzed the case where two arcs can be observed in the IS spectra, assuming both transport channels to be highly conductive (no transport resistance). In this case, we have shown that the first arc at low frequency is always associated with the dielectric relaxation while the second one is the drift-diffusion-recombination process and the size of both semicircles varies relatively with the dielectric relaxation resistance. In this case, the total resistance at zero frequency is always the recombination resistance. We have also shown how to extract the resistance of the dielectric relaxation and both chemical and dielectric capacitances from such IS spectra. Subsequently, we have analyzed the effect of a distribution of dielectric relaxation

dx.doi.org/10.1021/jp5062144 | J. Phys. Chem. C 2014, 118, 18983−18991

lifetimes and have shown that the chemical capacitance can be shifted at much higher frequencies than for a single relaxation lifetime. In this configuration, only one elliptic arc can be observed, which is associated with the dielectric relaxation. Finally, the consideration of current sources produces some exotic features in the form of inductive (or negative capacitance) effect that have been previously observed in perovskite solar cells.

■ ASSOCIATED CONTENT

Supporting Information

The procedure for the calculation of the complex impedance of the general transmission line, the MATLAB program implemented to calculate the IS spectra, the calculation of the impedance Z_0, the calculation of $R_{\|}$, τ_1, and τ_2. This material is available free of charge via the Internet at http://pubs.acs.org.

■ AUTHOR INFORMATION

Corresponding Author

*E-mail: bisquert@uji.es.

Notes

The authors declare no competing financial interest.

■ ACKNOWLEDGMENTS

The research leading to these results has received funding from MINECO of Spain under project MAT2013-47192-C3-1-R, and the European Union Seventh Framework Program [FP7/2007-2013] under grant agreement 316494.

■ REFERENCES

(1) Fabregat-Santiago, F.; Bisquert, J.; Garcia-Belmonte, G.; Boschloo, G.; Hagfeldt, A. Impedance Spectroscopy Study of the Influence of Electrolyte Conditions in Parameters of Transport and Recombination in Dye-Sensitized Solar Cells. *Sol. Energy Mater. Sol. Cells* **2005**, *87*, 117−131.

(2) Garcia-Belmonte, G.; Guerrero, A.; Bisquert, J. Elucidating Operating Modes of Bulk-Heterojunction Solar Cells from Impedance Spectroscopy Analysis. *J. Phys. Chem. Lett.* **2013**, *4*, 877−886.

(3) Mora-Seró, I.; Garcia-Belmonte, G.; Boix, P. P.; Vázquez, M. A.; Bisquert, J. Impedance Characterisation of Highly Efficient Silicon Solar Cell under Different Light Illumination Intensities. *Energy Environ. Sci.* **2009**, *2*, 678−686.

(4) Bisquert, J. Theory of the Impedance of Electron Diffusion and Recombination in a Thin Layer. *J. Phys. Chem. B* **2002**, *106*, 325−333.

(5) Bisquert, J.; Mora-Sero, I.; Fabregat-Santiago, F. Diffusion-Recombination Impedance Model for Solar Cells with Disorder and Nonlinear Recombination. *ChemElectroChem* **2013**, *1*, 289−296.

(6) Bisquert, J. Chemical Capacitance of Nanostructured Semiconductors: Its Origin and Significance for Heterogeneous Solar Cells. *Phys. Chem. Chem. Phys.* **2003**, *5*, 5360−5364.

(7) Fabregat-Santiago, F.; Garcia-Belmonte, G.; Mora-Seró, I.; Bisquert, J. Characterization of Nanostructured Hybrid and Organic Solar Cells by Impedance Spectroscopy. *Phys. Chem. Chem. Phys.* **2011**, *13*, 9083−9118.

(8) Wang, Q.; Ito, S.; Grätzel, M.; Fabregat-Santiago, F.; Mora-Seró, I.; Bisquert, J.; Bessho, T.; Imai, H. Characteristics of High Efficiency Dye-Sensitized Solar Cells. *J. Phys. Chem. B* **2006**, *110*, 19406−19411.

(9) Fabregat-Santiago, F.; Bisquert, J.; Palomares, E.; Otero, L.; Kuang, D.; Zakeeruddin, S. M.; Grätzel, M. Correlation Between Photovoltaic Performance and Impedance Spectroscopy of Dye-Sensitized Solar Cells based on Ionic Liquids. *J. Phys. Chem. C* **2007**, *111*, 6550−6560.

(10) Bisquert, J.; Marcus, R. A. Device Modeling of Dye-Sensitized Solar Cells. *Top. Curr. Chem.* **2013**, DOI: 10.1007/128_2013_471.

(11) Kim, H.-S.; Im, S. H.; Park, N.-G. Organolead Halide Perovskite: New Horizons in Solar Cell Research. *J. Phys. Chem. C* **2014**, *118*, 5615−5625.

(12) Lee, M. M.; Teuscher, J.; Miyasaka, T.; Murakami, T. N.; Snaith, H. J. Efficient Hybrid Solar Cells Based on Meso-Superstructured Organometal Halide Perovskites. *Science* **2012**, *338*, 643−647.

(13) Kim, H.-S.; Lee, C.-R.; Im, J.-H.; Lee, K.-B.; Moehl, T.; Marchioro, A.; Moon, S.-J.; Humphry-Baker, R.; Yum, J.-H.; Moser, J. E.; Grätzel, M.; Park, N.-G. Lead Iodide Perovskite Sensitized All-Solid-State Submicron Thin Film Mesoscopic Solar Cell with Efficiency Exceeding 9%. *Sci. Rep.* **2012**, *2*, 591.

(14) Kojima, A.; Teshima, K.; Shirai, Y.; Miyasaka, T. Organometal Halide Perovskites as Visible-Light Sensitizers for Photovoltaic Cells. *J. Am. Chem. Soc.* **2009**, *131*, 6050−6051.

(15) Gonzalez-Pedro, V.; Juarez-Perez, E. J.; Arsyad, W.-S.; Barea, E. M.; Fabregat-Santiago, F.; Mora-Sero, I.; Bisquert, J. General Working Principles of $CH_3NH_3PbX_3$ Perovskite Solar Cells. *Nano Lett.* **2014**, *14*, 888−893.

(16) Kim, H.-S.; Mora-Sero, I.; Gonzalez-Pedro, V.; Fabregat-Santiago, F.; Juarez-Perez, E. J.; Park, N.-G.; Bisquert, J. Mechanism of Carrier Accumulation in Perovskite Thin-Absorber Solar Cells. *Nature Commun.* **2013**, *4*, 2242.

(17) Sanchez, R. S.; Gonzalez-Pedro, V.; Lee, J.-W.; Park, N.-G.; Kang, Y. S.; Mora-Sero, I.; Bisquert, J. Slow Dynamic Processes in Lead Halide Perovskite Solar Cells. Characteristic Times and Hysteresis. *J. Phys. Chem. Lett.* **2014**, *5*, 2357−2363.

(18) Frost, J. M.; Butler, K. T.; Brivio, F.; Hendon, C. H.; Van Schilfgaarde, M.; Walsh, A. Atomistic Origins of High-Performance in Hybrid Halide Perovskite Solar Cells. *Nano Lett.* **2014**, *14*, 2584−2590.

(19) Juarez-Perez, E. J.; Sanchez, R. S.; Badia, L.; Garcia-Belmonte, G.; Gonzalez-Pedro, V.; Kang, Y. S.; Mora-Sero, I.; Bisquert, J. Photoinduced Giant Dielectric Constant in Lead Halide Perovskite Solar Cells. *J. Phys. Chem. Lett.* **2014**, *5*, 2390−2394.

(20) Sah, C.-T. The Equivalent Circuit Model in Solid State Electronics—Part I: The Single Energy Level Defect Centers. *Proc. IEEE* **1967**, *55*, 654.

(21) Barker, G. C. Aperiodic Equivalent Circuits for the Electrolyte Solution. The Ideally Polarizable Electrode and the Ion and its Atmosphere. *J. Electroanal. Chem.* **1973**, *41*, 201.

(22) Brumleve, T. R.; Buck, R. P. Numerical Solution of the Nernst−Planck and Poisson Equation System with Applications to Membrane Electrochemistry and Solid State Physics. *J. Electroanal. Chem.* **1978**, *90*, 1.

(23) Brumleve, T. R.; Buck, R. P. Transmission Line Equivalent Circuit Models for Electrochemical Impedances. *J. Electroanal. Chem.* **1981**, *126*, 73.

(24) Böttcher, C. J. F.; Bordewijk, P. *Theory of Electric Polarization*; Elsevier: Amsterdam, 1978; Vol. *II*.

(25) Jonscher, A. K. *Dielectric Relaxation in Solids*; Chelsea Dielectrics Press: London, 1983.

(26) Bertoluzzi, L.; Boix, P. P.; Mora-Sero, I.; Bisquert, J. Theory of Impedance Spectroscopy of Ambipolar Solar Cells with Trap-Mediated Recombination. *J. Phys. Chem. C* **2014**, *118*, 16574−16580.

(27) Pitarch, A.; Garcia-Belmonte, G.; Mora-Seró, I.; Bisquert, J. Electrochemical Impedance Spectra for the Complete Equivalent Circuit of Diffusion and Reaction Under Steady-State Recombination Current. *Phys. Chem. Chem. Phys.* **2004**, *6*, 2983−2988.

(28) Jamnik, J.; Maier, J. Generalised Equivalent Circuits for Mass and Charge Transport: Chemical Capacitance and its Implications. *Phys. Chem. Chem. Phys.* **2001**, *3*, 1668−1678.

(29) Juarez-Perez, E. J.; Wussler, M.; Fabregat-Santiago, F.; Lakus-Wollny, K.; Mankel, E.; Mayer, T.; Jaegermann, W.; Mora-Sero, I. Role of the Selective Contacts in the Performance of Lead Halide Perovskite Solar Cells. *J. Phys. Chem. Lett.* **2014**, *5*, 680−685.

(30) Ripolles-Sanchis, T.; Guerrero, A.; Bisquert, J.; Garcia-Belmonte, G. Diffusion-Recombination Determines Collected Current and Voltage in Polymer:Fullerene Solar Devices. *J. Phys. Chem. C* **2012**, *116*, 16925−16933.

(31) Garcia-Belmonte, G.; Bueno, P. R.; Fabregat-Santiago, F.; Bisquert, J. Relaxation Processes in the Coloration of Amorphous WO_3 Thin Films Studied by Combined Impedance and Electro-Optical Measurements. *J. Appl. Phys.* **2004**, *96*, 853−859.
(32) Bueno, P. R.; Cassia-Santos, M. R.; Leite, E. R.; Longo, E.; Bisquert, J.; Garcia-Belmonte, G.; Fabregat-Santiago, F. Nature of the Schottky Type Barrier of Highly Dense SnO_2 Systems Displaying Nonohmic Behaviour. *J. Appl. Phys.* **2000**, *88*, 6545−6548.
(33) Mora-Seró, I.; Bisquert, J.; Fabregat-Santiago, F.; Garcia-Belmonte, G.; Zoppi, G.; Durose, K.; Proskuryakov, Y. Y.; Oja, I.; Belaidi, A.; Dittrich, T.; et al. Implications of the Negative Capacitance Observed at Forward Bias in Nanocomposite and Polycrystalline Solar Cells. *Nano Lett.* **2006**, *6*, 640−650.